Factors Governing the Enhanced Reactivity of Five-Membered Cyclic Phosphate Esters

Nai-yuan Chang[†] and Carmay Lim*[,†,‡]

Contribution from the Institute of Biomedical Sciences, Academia Sinica, and Department of Chemistry, National Tsing-Hua University Taipei, Taiwan 11529, Republic of China

Received August 25, 1997. Revised Manuscript Received January 2, 1998

Abstract: Ab initio calculations and continuum dielectric methods have been employed to map out the lowest activation free-energy profiles for the alkaline hydrolysis of a five-membered cyclic phosphate, methyl ethylene phosphate (MEP), its acyclic analog, trimethyl phosphate (TMP), and its six-membered ring counterpart, methyl propylene phosphate (MPP). The rate-limiting step for the three reactions was found to be hydroxyl ion attack at the phosphorus atom of the triester. By performing constrained optimization along the reaction coordinate, defined as the phosphorus to incoming hydroxyl oxygen distance, and computing the solvation free energies of the resulting stationary points, the rate-limiting transition states have been relocated in solution. Dihedral ring constraints in the five-membered ring leading to a more solvent-exposed hydroxyl group and, thus, better solvation of the cyclic transition state compared to its acyclic counter-part was found to be the dominant factor governing the rate enhancement of cyclic MEP relative to acyclic TMP alkaline hydrolysis. However, both ground-state destabilization of MEP relative to MPP, due to ring strain, and transition-state stabilization of the five-membered cyclic phosphate transition state relative to its six-membered ring analog, due to the differential location of the transition states in solution, were found to contribute to the enhanced rates of alkaline hydrolysis of five-membered ring MEP compared to six-membered ring MPP.

Introduction

Phosphate esters are ubiquitous in living systems and have been selected by evolution for biochemical transformations.[1,2] Due to the important biological roles of phosphates,[2] there have been numerous studies of phosphate esters both in solution[3,4] as well as in the gas phase.[5−7] The pioneering studies by Westheimer and co-workers[3,4,8−11] have shown that the hydrolyses in acid or base of five-membered cyclic esters of phosphoric or phosphonic acids proceed much faster than the hydrolyses of their acyclic analogs. For example, the rate of alkaline hydrolysis of methyl ethylene phosphate (MEP) at 298 K exceeds that of trimethyl phosphate (TMP) by 4.7×10^5, corresponding to an activation free-energy difference of 7.8 kcal/mol.[3,12] In sharp contrast, the rates of hydrolysis of six- and seven-membered cyclic phosphates are comparable to those of acyclic phosphates.[3] The experimental studies have also provided indirect evidence for the formation of a trigonal bipyramidal pentacovalent (TBP) intermediate under certain reaction conditions,[3,4,13] which was subsequently confirmed by theoretical studies.[14,15]

Aksnes and Bergesen[16] have obtained the rate constants for the alkaline hydrolysis of cyclic and open chain phosphinates, phosphonates, and phosphates as well as their temperature dependence. The activation energy and entropy for the alkaline hydrolysis of ethyl propylphostonate (ethylene phosphate with one ring oxygen) are 11.7 ± 1 kcal/mol and −17 cal mol^{-1} deg^{-1}, respectively, whereas those for its acyclic analogue, diethyl ethyl phosphonate, are 14.0 ± 0.5 kcal/mol and −34 cal mol^{-1} deg^{-1}.[16] From these activation parameters, they concluded that the different rates of hydrolysis of the various phosphoryl esters were chiefly due to different entropies of activation. Kluger and Taylor[12] have determined the temperature dependence of the rates of alkaline hydrolysis of ethyl and methyl esters of ethylene phosphate and propylphostonate. The differences in activation enthalpies of the cyclic esters and the corresponding acyclic esters were 6−8 kcal/mol, whereas differences in activation entropies were less than 1 cal mol^{-1} deg^{-1} for the methyl esters and about 8 cal mol^{-1} deg^{-1} for the ethyl esters. In particular, they obtained an activation entropy for ethyl propylphostonate of −27 cal mol^{-1} deg^{-1} and an activation enthalpy of 7.6 kcal/mol, in contrast to the values reported by Aksnes and Bergensen.[16] They concluded that the rate acceleration of cyclic phosphate esters was due to enthalpic factors and not to entropic effects.

Several factors have been put forth to explain the large rate difference between five-membered cyclic phosphates and their

[†] National Tsing-Hua University.
[‡] Academia Sinica.

(1) Stryer, L. *Biochemistry*; W. H. Freeman: New York, 1995.
(2) Westheimer, F. H. *Science* **1987**, *235*, 1173−1178.
(3) Westheimer, F. H. *Acc. Chem. Res.* **1968**, *1*, 70−78.
(4) Thatcher, G. R. J.; Kluger, R. *Adv. Phys. Org. Chem.* **1989**, *25*, 99.
(5) Asubiojo, O. I.; Brauman, J. I.; Levin, R. H. *J. Am. Chem. Soc.* **1977**, *99*, 7707−7708.
(6) Hodges, R. V.; Sullivan, S. A.; Beauchamp, J. L. *J. Am. Chem. Soc.* **1980**, *102*, 935−938.
(7) Lum, R. C.; Grabowski, J. J. *J. Am. Chem. Soc.* **1992**, *114*, 8619−8627.
(8) Haake, P. C.; Westheimer, F. H. *J. Am. Chem. Soc.* **1961**, *83*, 1102−1109.
(9) Cox, J. R., Jr.; Ramsay, B. *Chem. Rev.* **1964**, *64*, 317.
(10) Kluger, R.; Covitz, F.; Dennis, E.; Williams, L. D.; Westheimer, F. H. *J. Am. Chem. Soc.* **1969**, *91*, 6066−6072
(11) Kluger, R.; Taylor, S. D. *J. Am. Chem. Soc.* **1991**, *113*, 5714.
(12) Kluger, R.; Taylor, S. D. *J. Am. Chem. Soc.* **1990**, *112*, 6669−6671.
(13) Kluger, R.; Thatcher, G. R. J. *J. Org. Chem.* **1986**, *51*, 207−212.
(14) Lim, C.; Tole, P. *J. Phys. Chem.* **1992**, *96*, 5217−5219.
(15) Tole, P.; Lim, C. *J. Phys. Chem.* **1993**, *97*, 6212−6219.
(16) Aksnes, G.; Bergesen, K. *Acta Chem. Scand.* **1966**, *20*, 2508−2514.

S0002-7863(97)02980-6 CCC: $15.00
Published on Web 02/24/1998

acyclic and six-membered ring counterparts. Ring strain, resulting in destabilization of the five-membered cyclic phosphate relative to the TBP rate-limiting transition state of the hydrolysis reaction, was originally and commonly assumed to be the chief driving force for the enhanced rates of ring cleavage.[8,17] Inherent in the ring strain hypothesis is the assumption that (i) the transition states for hydrolysis of both the five-membered cyclic and acyclic species are free of strain; (ii) the rate acceleration arises from ground-state destabilization (as opposed to transition-state stabilization) of the five-membered cyclic phosphate compared to its acyclic analog; and (iii) ring strain and its relief are enthalpic, not entropic, phenomena. Support for the ring strain hypothesis was provided by the higher heats of hydrolysis of five-membered cyclic phosphate esters relative to their acyclic counterparts and the observation that the O−P−O angle of five-membered ring phosphate triesters (98°) was significantly smaller than that (102−108°) observed for acyclic esters.[18] For MEP, the heat of hydrolysis exceeded that of dimethyl hydroxyethyl phosphate by 5.5−5.9 kcal/mol,[19,20] which is ca. 2 kcal/mol less than the activation enthalpy difference of 7.8 kcal/mol between the alkaline hydrolyses of MEP and TMP.[20] This discrepancy was attributed to steric crowding in the acyclic TBP transition state relative to that in the cyclic transition state, causing the former to be higher in energy than the latter (see ref 20, Figure 2). Thus, it was concluded that ring strain provided most, but not all, of the explanation for the rapid reaction of MEP.

Gorenstein and co-workers[21] have performed molecular orbital calculations to examine stereoelectronic effects in the hydrolyses of five-membered ring phosphate esters. The geometries of various conformational isomers of TBP neutral and dianionic dimethoxy phosphoranes were partially optimized using semiempirical (CNDO/2) and ab initio (HF/STO-3G) methods. Although Gorenstein and co-workers[21] did not carry out calculations on cyclic compounds, they proposed that most of the stabilization of the cyclic versus the acyclic transition states, which is not accounted for by strain energy, stems from orbital stereoelectronic effects in the TBP transition state of the cyclic species. Such effects would imply a rate differential due to a smaller entropy of activation for the cyclic species, which would not be consistent with the negligible differences in the activation entropies of cyclic five-membered phosphates relative to their acyclic counterparts (see above).[12,20] Furthermore, stereoelectronic effects would disfavor exocyclic cleavage of MEP in a strong base relative to endocyclic cleavage; however, significant amounts of exocyclic cleavage products were found in the strong alkaline hydrolysis of MEP (pH > 13).[10,13] More recent ab initio calculations of TBP transition states and intermediates of phosphate and phosphoamidate esters have shown that stereoelectronic effects do not seem to play a significant role in enhancing the reactivity of five-membered cyclic esters relative to their six-membered or acyclic analogs.[22,23]

Karplus and co-workers have carried out theoretical studies comparing the rates of hydrolysis of five-membered cyclic ethylene phosphate, $(EP)^-$, relative to its acyclic counterpart, dimethyl phosphate, $(DMP)^-$.[24] The energy profile for $(OH)^-$ attack of $(DMP)^-$ was determined by ab initio methods, and the solvation free energies of the reactants and transition states were calculated with the finite-difference linearized Poisson−Boltzmann equation method. They showed that although there is ring strain in the ground state of the cyclic reactant, it does not contribute to the rate acceleration. Furthermore, they showed that most of the rate acceleration observed in solution arises from differential solvation of the transition states, which, in turn, is dominated by the electric polarization associated with the hydroxy oxygen. This has been confirmed by the PM3-SM3 method,[25] which allows the solvent to polarize the gas-phase charge distribution of the ground states and rate-limiting transition states.

Note that solvation-effect calculations of dianionic species such as the rate-limiting transition states formed during the hydrolysis of ethylene phosphate and dimethyl phosphate are subject to large uncertainties and may not yield quantitatively reliable results. Furthermore, dianionic pentacovalent phosphorane intermediates that are unstable in the gas phase[26] may exist in solution. Although theoretical studies have been carried out on five-membered ring phosphates and their acyclic analogs,[14,15,24,27] there have been no detailed calculations (to our knowledge) on six-membered ring phosphates. To elucidate the driving forces behind the rate enhancement of cyclic five-membered ring phosphate, we chose to study the gas-phase and solution reactions of neutral triesters: MEP, its acyclic analog TMP, and its six-membered ring phosphate counterpart, methyl propylene phosphate (MPP). These triesters provide optimal models since there is a wealth of experimental solution data,[3,4,16] especially for MEP and TMP, and the gas-phase reactions of several anions with TMP have been studied.[5−7] The availability of such experimental data is critical for calibrating the ab initio and solvation free-energy calculations. Furthermore, since solvation free energies of monoanionic phosphates are much smaller than those of dianionic phosphates, errors in computing the former will likewise be smaller than uncertainties in computing the latter.

Ab initio calculations of the gas-phase activation free-energy profiles of the nucleophilic addition of $(OH)^-$, $(CH_3O)^-$ and F^- to TMP have been calibrated against gas-phase experimental data.[27] In this work, ab initio calculations at the same theory level as those performed for the TMP + $(OH)^-$ reaction have been carried out to determine the activation free-energy profiles for the nucleophilic addition of hydroxide to the phosphorus atom of MEP[14,15] and MPP. Subsequently, two different solvation models have been employed to determine the effect of solvent on the gas-phase activation free-energy profiles. In particular, relocation of the rate-limiting transition state in solution for each of the three reactions studied has been determined. Details of the calculations are described in the Methods section. The reaction mechanisms and rate-limiting transition states for the alkaline hydrolyses of TMP, MEP, and MPP are presented in the Results. In the Discussion, the results are first calibrated against available experimental data such as product distribution and relative activation free energies. The

(17) Emsley, J.; Hall, D. *The Chemistry of Phosphorus*; John Wiley and Sons: New York, 1976.
(18) Gerlt, J. A.; Westheimer, F. H.; Sturtevant, J. M. *J. Biol. Chem.* **1975**, *250*, 5059.
(19) Kaiser, E. T.; Panar, M.; Westheimer, F. H. *J. Am. Chem. Soc.* **1963**, *85*, 63.
(20) Taylor, S. D.; Kluger, R. *J. Am. Chem. Soc.* **1992**, *114*, 3067−3071.
(21) Gorenstein, D. G.; Luxon, B. A.; Findlay, J. B.; Momii, R. *J. Am. Chem. Soc.* **1977**, *99*, 4170.
(22) Tole, P.; Lim, C. In *The Anomeric Effect and Associated Stereoelectronic Effects*; Thatcher, G. R., Ed.; ACS Symposium Series No. 539; American Chemical Society: Washington, DC, 1993.
(23) Tole, P.; Lim, C. *J. Am. Chem. Soc.* **1994**, *116*, 3922−3931.
(24) Dejaegere, A.; Liang, X.; Karplus, M. *J. Chem. Soc., Faraday Trans.* **1994**, *90*, 1763−1770.
(25) Cramer, C. J.; Hawkins, G. D.; Truhlar, D. G. *J. Chem. Soc., Faraday Trans.* **1994**, *90*, 1802−1804.
(26) Lim, C.; Karplus, M. *J. Am. Chem. Soc.* **1990**, *112*, 572−5873.
(27) Chang, N. Y.; Lim, C. *J. Phys. Chem.* **1997**, *101*, 8706−8713.

Table 1. Atomic Radii (Å) Used in Solvation Free-Energy Calculations

	atom				
	P	O	C	H	H(O)
CDM	2.15	1.77	1.80	1.47	0.23
PSGVB/DelPhi	2.07	1.60	1.90	1.15	1.15

individual factors governing the rate acceleration of five-membered cyclic MEP relative to its acyclic analog, TMP, and six-membered ring counterpart, MPP, are identified. The key results are summarized in the Conclusions.

Methods

Gas-Phase Free Energies. The gas-phase reaction profiles were initially explored using the Gaussian 94 program[28] at the Hartree−Fock (HF) level with a 6-31+G* basis set, unless stated otherwise. The nature of each transition state was verified by a single imaginary frequency and an intrinsic reaction coordinate[29−31] calculation leading to the expected ground state and products. The correlation energy was estimated with second-order Møller−Plesset theory and the 6-31+G* basis set using fully optimized HF/6-31+G* geometries. To assess the reliability of the MP2/6-31+G*//HF/6-31+G* calculations, certain transition states were reoptimized at the MP2/6-31+G* level and the correlation energy was computed using increasing basis sets and levels of theory (see Results and Discussion). The frozen-core approximation (rather than all electrons) was employed in all MP2 correlation calculations.

To determine the thermodynamic parameters, vibrational frequencies were computed for the fully optimized structures of the stationary points along the reaction profile. The HF/6-31+G* frequencies were scaled by an empirical factor of 0.8929 to correct for any errors that may arise from anharmonicity in the potential energy surface, inadequate basis sets, and the neglect of electron correlation.[32] The entropy (S_{vib}), zero-point energy (ZPE), and vibrational energy (E_{vib}) were calculated from the frequencies and geometries according to standard statistical mechanical formulas.[33] The rotational (E_{rot}) and translational (E_{trans}) energies and the work term (PV) were treated classically. Addition of the energetic and entropic corrections to the MP2/6-31+G*//HF/6-31+G* activation energies gave the gas-phase free energy barriers, $\Delta G^{\ddagger}_{gas}$.

Solvation Free Energies. Solvation free energies of the stationary points were estimated by solving the Poisson equation using finite difference methods. The calculations employed a 71 × 71 × 71 lattice centered on the phosphorus with a grid spacing of 0.25 Å.[34−36] The low-dielectric region of the solute was defined as the region inaccessible to contact by a 1.4 Å sphere rolling over a surface defined by the effective solute radii, which were taken from the CHARMM[37] (version 22) van der Waals radii (see Table 1). This region was assigned a dielectric constant of 2 to account for the electronic polarizability of the solute. The (highest level) ab initio geometries and CHelpG[38] partial atomic charges, which were assumed to be the same in vacuum and solution, were employed. The difference between the electrostatic potential calculated in solvent and vacuum, characterized by a dielectric constant of 80 and 1, respectively, yielded the electrostatic solvation free energy. The latter will be refered to as CDM ΔG_s.

To allow for the change in molecular charge distribution in going from the gas phase to solution, solvation free energies were also estimated using the PSGVB program,[39,40] which combines high-level ab initio quantum mechanical calculations with a continuum description of the solvent. First, a gas-phase quantum mechanical calculation was performed using PSGVB. Next, a set of atomic point charges was obtained by fitting the long-range Coulombic field from the wave function using a least-squares criterion. These charges were then employed by the program DelPhi[41] to solve the Poisson equation. The DelPhi calculations employed the same finite difference formulation described above except that the internal dielectric constant was set equal to 1, as molecular polarizability was treated explicitly in the quantum mechanical calculations. Furthermore, the DelPhi calculations used a different set of atomic radii parameters (see Table 1). The reaction field in a continuum solvent model, defined as the difference field between a uniform dielectric Poisson calculation and a two-dielectric Poisson calculation, can be exactly represented as due to a set of charges at the dielectric boundary, calculated as the divergence of the field at the surface. This set of point charges was calculated in DelPhi and subsequently employed in PSGVB to solve the wave function in the presence of the electrostatic field of the point charges. The PSGVB and DelPhi calculations were iterated until the total energy of two iterations agreed to within a preset tolerance. The electrostatic solvation free energy was then obtained as the difference between the gas-phase and solution-phase quantum chemical energies. This is referred to as PSGVB ΔG_s.

Solution Free Energy Barrier. The solution free-energy barrier, $\Delta G^{\ddagger}_{sln}$, from A to B can be calculated from the thermodynamic cycle

$$\begin{array}{ccc} & \overset{\Delta G^{\ddagger}_{gas}}{\longrightarrow} & \\ \mathrm{A(gas)} & & \mathrm{B(gas)} \\ \downarrow \Delta G_s(\mathrm{A}) & & \downarrow \Delta G_s(\mathrm{B}) \\ \mathrm{A(sln)} & \underset{\Delta G^{\ddagger}_{sln}}{\longrightarrow} & \mathrm{B(sln)} \end{array}$$

where $\Delta G^{\ddagger}_{gas}$ is the gas-phase free-energy barrier and the ΔG_s values are solvation free energies. Thus, the solution free energy barrier $\Delta G^{\ddagger}_{sln}$ (A → B) is given by

$$\Delta G^{\ddagger}_{sln} = \Delta G^{\ddagger}_{gas} + \Delta G_s(\mathrm{B}) - \Delta G_s(\mathrm{A}) \qquad (1)$$

Results

Tables 2−4 summarize the gas-phase thermodynamic parameters and solvation free energies computed using the continuum dielectric method, whereas Figures 1−3 illustrate the relative MP2/6-31+G*//HF/6-31+G* activation free-energy profiles and their changes upon solvation for the reactions of $(OH)^-$ at the phosphorus atom of TMP, MEP and MPP, respectively. The zero of energy corresponds to the reactants at infinite separation in the gas phase.

1. The Reaction of $(OH)^-$ with TMP. The possible reaction pathways for the gas-phase reaction of $(OH)^-$ at the phosphorus and carbon sites of TMP have been presented in

(28) Frisch, M. J.; Trucks, G. W.; Schlegel, H. B.; Gill, P. M. W.; Johnson, B. G.; Robb, M. A.; Cheeseman, J. R.; Petersson, T.; Keith, G. A.; Montgomery, J. A.; Raghavachari, K.; Al-Laham, M. A.; Zakrzewski, V. G.; Ortiz, J. V.; Foresman, J. B.; Cioslowski, J.; Stefanov, B. B.; Nanayakkara, A.; Challacombe, M.; Peng, C. Y.; Ayala, P. Y.; Chen, W.; Wong, M. W.; Andres, J. L.; Replogle, E. S.; Gomperts, R.; Martin, R. L.; Fox, D. J.; Binkley, J. S.; Defrees, D. J.; Baker, J.; Stewart, J. P.; Head-Gordon, M.; Gonzalez, C.; Pople, J. A. *Gaussian 94*; Gaussian Inc.: Pittsburgh, PA, 1995.

(29) Fukui, K. *Acc. Chem. Res.* **1981**, *14*, 363−368.

(30) Gonzalez, C.; Schegel, H. B. *J. Chem. Phys.* **1989**, *90*, 2154-2161.

(31) Gonzalez, C.; Schegel, H. B. *J. Phys. Chem.* **1990**, *94*, 5523−5527.

(32) Hehre, W. J.; Radom, L.; Schleyer, P. v. R.; Pople, J. A. *Ab Initio Molecular Orbital Theory*; John Wiley and Sons: New York, 1986.

(33) McQuarrie, D. A. *Statistical Mechanics*; Harper and Row: New York, 1976.

(34) Warwicker, J.; Watson, H. C. *J. Mol. Biol.* **1982**, *157*, 671−679.

(35) Gilson, M. K.; Honig, B. H. *Proteins: Struct., Funct., Genet.* **1988**, *4*, 7−18.

(36) Lim, C.; Bashford, D.; Karplus, M. *J. Phys. Chem.* **1991**, *95*, 5610−5620.

(37) Brooks, B. R.; Bruccoleri, R. D.; Olafson, B. O.; States, D. J.; Swaminathan, S.; Karplus, M. *J. Comput. Chem.* **1983**, *4*, 187−217.

(38) Chirlian, L. E.; Francl, M. M. *J. Comput. Chem.* **1987**, *8*, 894.

(39) Friesner, R. *Ann. Rev. Phys. Chem.* **1991**, *42*, 34−1362.

(40) Ringnalda, M.; Langlois, J. M.; Murphy, R. B.; Greeley, B. H.; Cortis, C.; Russo, T. V.; Marten, B., Jr.; Donnelly, R. E.; Pollard, W. T.; Cao, Y.; Muller, R. P.; Mainz, D. T.; Wright, J. R.; Miller, G. H., III; Goddard, W. A.; Friesner, R. A. *PSGVB*; Schrodinger Inc.: New York, 1996.

(41) Nicholls, A.; Honig, B. *J. Comput. Chem.* **1991**, *12*, 435−445.

Scheme 1. Schematic Diagram Depicting Fully Optimized HF/6-31+G* Structures for the Reaction of $(OH)^-$ at the Phosphorus of TMP (TMP(P)) (Not All Transition States and Intermediates along the Pathways Are Depicted for the Sake of Clarity.)

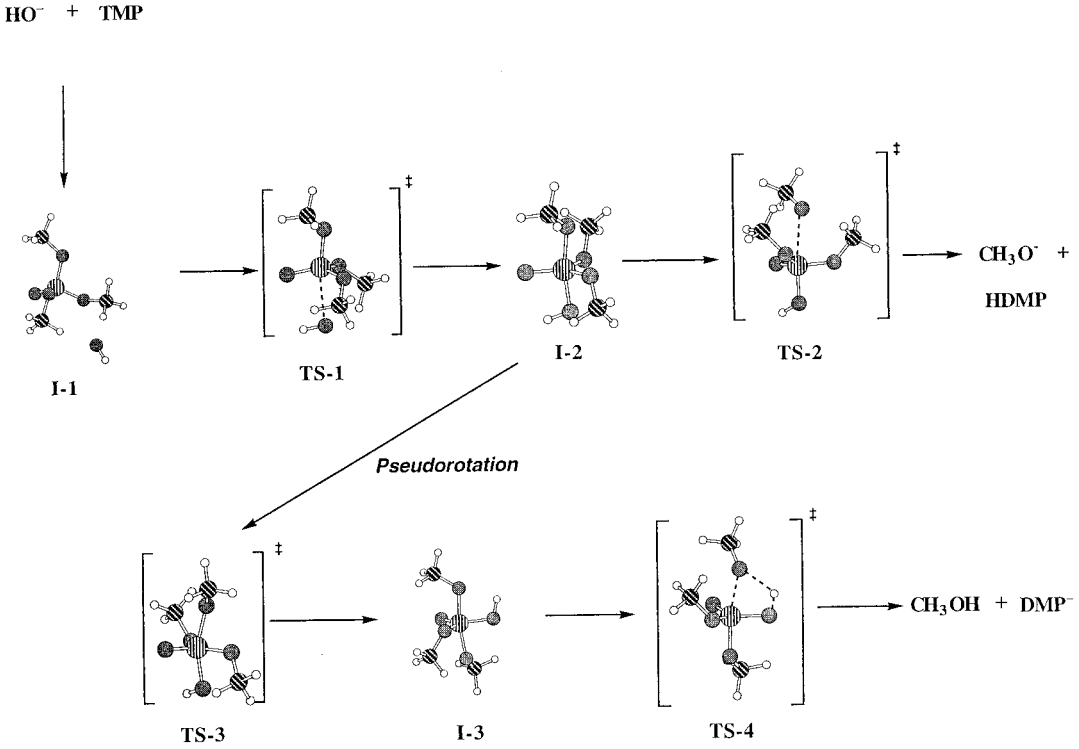

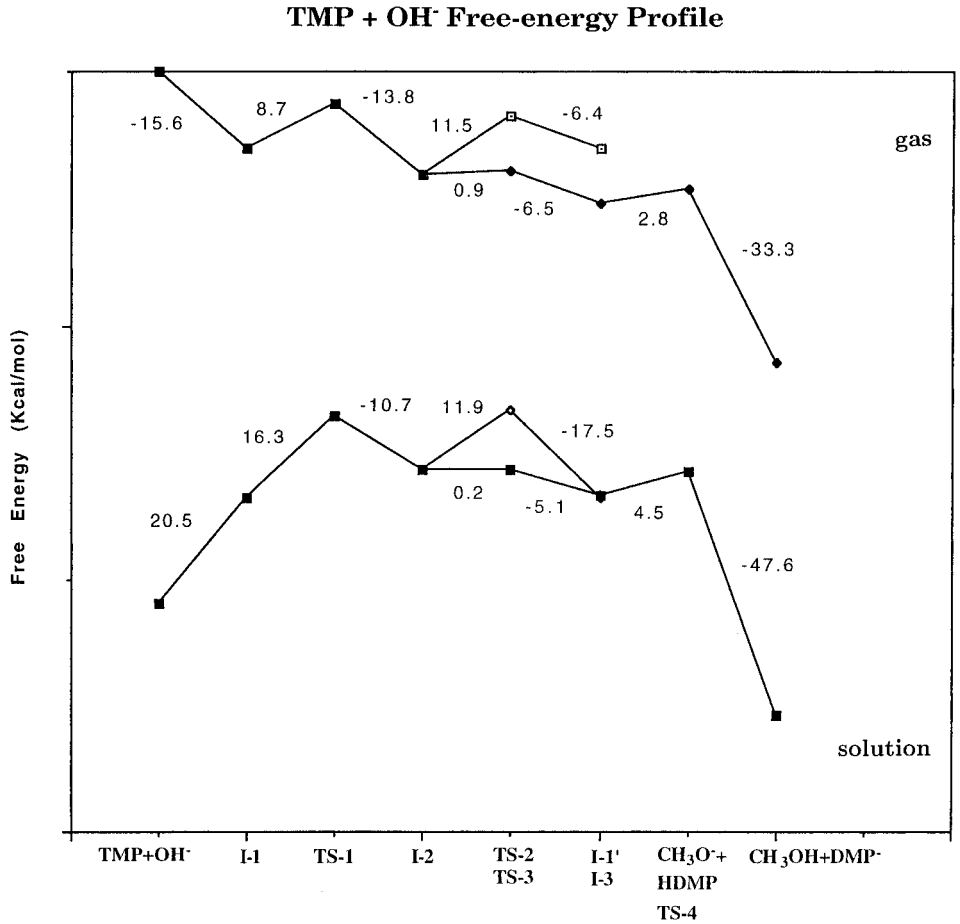

Figure 1. Relative MP2/6-31+G*//HF/6-31+G* activation free-energy profile for the gas-phase reaction of $(OH)^-$ with TMP (top) and the change in profile upon solvation (bottom). The zero of energy corresponds to the reactants at infinite separation. The numbers correspond to the free-energy differences of subsequent points. The free energy of the ion−dipole complex, $(CH_3O)^-\cdots$HDMP, which was not computed, was assumed to be similar to that of **I-1**.

Table 2. Relative Energies, Entropies, and Free Energies for Reaction 1 at 298 K with Respect to the Reactants Separated at Infinity in the Gas Phase (All Energies Are Reported to 1 Decimal Place in kcal/mol)

species	ΔE^a	ΔZPE^b	$\Delta E_{TRV}{}^c$	$T\Delta S_{TRV}{}^c$	$\Delta G_{gas}{}^d$	$\Delta G_s{}^e$	$\Delta G_{sln}{}^f$
TMP + OH^-	0.0	0.0	0.0	0.0	0.0	−105.0	0.0
I-1	−26.0	1.2	1.4	−8.3	−15.6	−68.9	20.5
I-2	−37.3	3.3	2.3	−11.6	−20.7	−58.3	26.0
I-3	−43.7	3.6	2.5	−11.9	−26.3	−57.6	21.1
TS-1	−20.1	1.8	1.1	−10.9	−6.9	−61.4	36.7
TS-2	−21.2	1.3	0.6	−10.6	−9.2	−58.0	37.9
TS-3	−37.6	3.3	1.7	−13.3	−19.9	−59.0	26.2
TS-4	−38.5	2.5	1.4	−11.5	−23.6	−55.9	25.6
$(DMP)^-$ + MeOH	−57.6	1.5	0.7	1.5	−56.9	−70.2	−22.0

[a] From single-point MP2/6-31+G*//HF/6-31+G* calculations. [b] Zero-point energy contribution. [c] Both ΔE_{TRV} and ΔS_{TRV} include the translational, rotational, and vibrational contributions. [d] $\Delta G_{gas} = \Delta E + \Delta$ZPE $+ \Delta E_{TRV} + \Delta PV - T\Delta S_{TRV}$. [e] Solvation free energies computed using MP2/6-31+G* CHelpG charges and HF/6-31+G* geometry. [f] Solution free energies computed using eq 1.

Table 3. Relative Energies, Entropies, and Free Energies for Reaction 2 at 298 K with Respect to the Reactants Separated at Infinity in the Gas Phase (All Energies Are Reported to 1 Decimal Place in kcal/mol)[a]

species	ΔE	ΔZPE	ΔE_{TRV}	$T\Delta S_{TRV}$	ΔG_{gas}	ΔG_s	ΔG_{sln}
MEP + OH^-	0.0	0.0	0.0	0.0	0.0	−106.2	0.0
I-4	−15.2	0.0	0.4	−6.9	−8.6	−81.2	16.4
I-5	−51.6	3.4	2.5	−11.3	−35.1	−61.5	9.6
I-6	−52.8	3.5	2.5	−11.6	−35.9	−61.6	8.7
TS-5	−15.2	1.0	0.8	−9.6	−4.5	−72.6	29.1
TS-6	−48.4	2.6	1.5	−11.5	−33.4	−59.6	13.2
TS-7	−42.3	3.4	0.4	−11.3	−27.9	−66.5	11.8
TS-8	−39.7	1.6	0.8	−10.5	−27.4	−60.1	18.8
$(MHEP)^-$	−81.4	3.5	3.1	−9.6	−65.8	−60.0	−19.6
$(EP)^-$ + MeOH	−59.7	1.4	0.7	1.9	−59.6	−72.2	−25.6

[a] See the footnotes of Table 2.

our previous work.[27] Here, only the lowest gas-phase activation free-energy pathway for the nucleophilic addition of $(OH)^-$ to the phosphorus atom of TMP (denoted by TMP(P)) is depicted in Scheme 1 and Figure 1. When $(OH)^-$ approaches the phosphorus atom of TMP, an ion−dipole minimum (**I-1**) is initially formed. As the $P-O^H$ distance decreases, the two equatorial methoxy groups in **I-1** rotate toward the incoming $(OH)^-$ to minimize the electrostatic repulsion among the negatively charged hydroxyl oxygen and methoxy oxygens, forming a long-range distorted TBP transition state (**TS-1**) at a hydroxyl O−P distance of 2.56 Å. As the $P-O^H$ distance decreases further, a metastable pentacovalent TBP intermediate (**I-2**) was found, with an axial hydroxyl O−P bond length of 1.72 Å. Pseudorotation of **I-2**, which requires an activation free energy of only 0.9 kcal/mol, produces a more stable TBP intermediate (**I-3**) with the hydroxyl group equatorial. The latter undergoes cleavage of the axial P−O bond that is cis to the O−H bond with simultaneous proton transfer via **TS-4** to yield CH_3OH and $(DMP)^-$.

Figure 1 shows how the gas-phase activation free-energy profile is changed in solution. Solvation leads to the disappearance of the ion−dipole minimum, thus inducing an activation free-energy barrier of 37 kcal/mol (at the MP2/6-31+G*//HF/6-31+G* level, see Table 2) for reactants to **TS-1** in solution. The lowest free-energy pathway for the reaction of $(OH)^-$ with TMP(P) in solution is similar to that found in the gas phase; in particular, the rate-limiting transition state in the gas phase and solution is **TS-1**.

Table 4. Relative Energies, Entropies, and Free Energies for Reaction 3 at 298 K with Respect to the Reactants Separated at Infinity in the Gas Phase (All Energies Are Reported to 1 Decimal Place in kcal/mol)[a]

species	ΔE	ΔZPE	ΔE_{TRV}	$T\Delta S_{TRV}$	ΔG_{gas}	ΔG_s	ΔG_{sln}
MPP + OH^-	0.0	0.0	0.0	0.0	0.0	−105.9	0.0
I-7	−15.1	0.7	1.3	−6.8	−6.9	−77.4	21.6
I-8	−44.7	3.3	2.4	−11.6	−28.0	−58.9	19.0
I-9	−46.4	3.6	2.6	−11.9	−29.0	−59.3	17.6
TS-9	−13.4	1.2	0.7	−10.7	−1.3	−70.3	34.3
TS-10	−42.6	2.6	1.5	−11.9	−27.3	−57.5	21.1
TS-11	−33.7	2.2	1.2	−11.8	−19.2	−61.9	24.8
TS-12	−36.3	1.9	1.0	−11.1	−23.0	−58.2	24.7
$(MHPP)^-$	−78.1	3.4	3.1	−9.5	−62.8	−59.0	−16.0
PP^- + MeOH	−61.5	1.7	0.8	0.5	−59.6	−70.6	−24.3

[a] See the footnotes of Table 2.

2. The Reaction of $(OH)^-$ with MEP. The lowest gas-phase activation free energy pathway for the reaction of $(OH)^-$ at the phosphorus atom of MEP (denoted by MEP(P)) is illustrated in Scheme 2, and the effect of solvation is shown in Figure 2. The key difference between $(OH)^-$ attack at MEP(P) and TMP(P) is that the former does not yield a stable TBP intermediate with the hydroxyl group axial.[14,15] Hydroxyl attack of MEP(P) is concerted with pseudorotation to yield a TBP intermediate with the hydroxyl group equatorial. Another significant difference is that the pathway leading to the production of methanol is not the lowest activation free-energy pathway for the reaction of $(OH)^-$ at MEP(P), in contrast to that at TMP(P). Both in the gas phase and in solution, endocyclic cleavage of the **I-5** intermediate is kinetically more favorable than exocyclic cleavage of the **I-6** intermediate, yielding the ring-cleavage product, methyl hydroxyethyl phosphate $(MHEP)^-$.

3. The Reaction of $(OH)^-$ with MPP. Scheme 3 depicts the lowest gas-phase activation free-energy pathway for the reaction of $(OH)^-$ at the phosphorus atom of MPP (denoted by MPP(P)), while Figure 3 shows the effect of solvation. In the gas phase, the six-membered ring of MPP exists in three distinct conformations: chair, boat, and twist forms. Only the most stable chair form was considered here. As shown in Scheme 3 and Figure 3, the gas-phase and solution activation free-energy profiles for the alkaline hydrolysis of MPP are similar to those obtained for the $(OH)^-$ + MEP reaction. No TBP intermediate with the hydroxyl group axial was found as for the $(OH)^-$ + MEP reaction,[14] but in contrast to the $(OH)^-$ + TMP reaction. Geometry optimization at the HF/6-31+G* level with analytic force constants computed at each point failed to locate a TBP intermediate with an axial hydroxyl group and resulted in the pseudorotated TBP intermediate **I-8** with the hydroxyl group equatorial. In both MEP and MPP hydrolysis reactions, pseudorotation was found to be concurrent with $(OH)^-$ attack, implying that pseudorotation in these two cases is a fast process[15] rather than a slow one, as assumed by previous workers.[4,10] Another feature common to both $(OH)^-$ + MEP and $(OH)^-$ + MPP reactions is that endocyclic cleavage of the pseudorotated intermediate is kinetically more favorable than exocyclic cleavage, and the rate-limting step is formation of the long-range transition state. Note that as for the $(OH)^-$ + MEP reaction,[15] $(OH)^-$ attack opposite a ring oxygen via **TS-9** is favored over $(OH)^-$ attack opposite a methoxy oxygen via

Scheme 2. Schematic Diagram Depicting Fully Optimized HF/6-31+G* Structures for the Reaction of $(OH)^-$ at Phosphorus of MEP (MEP(P)) (Not All Transition States and Intermediates along the Pathways Are Depicted for the Sake of Clarity.)

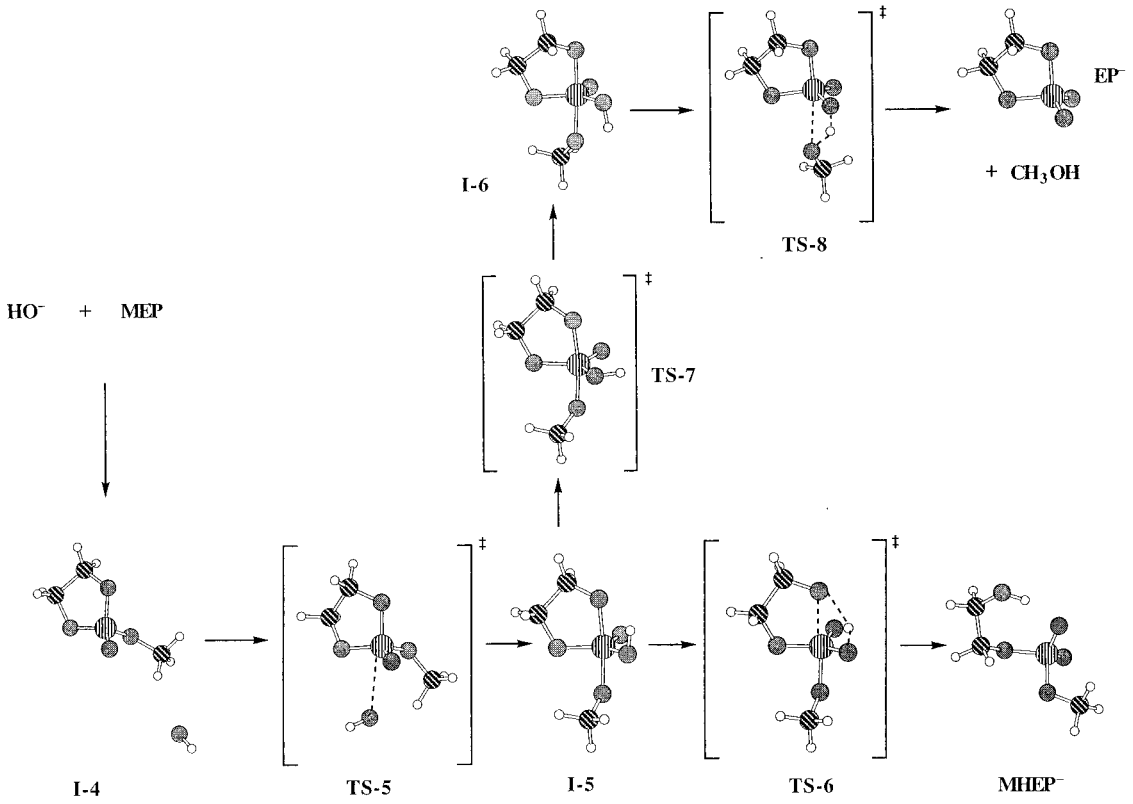

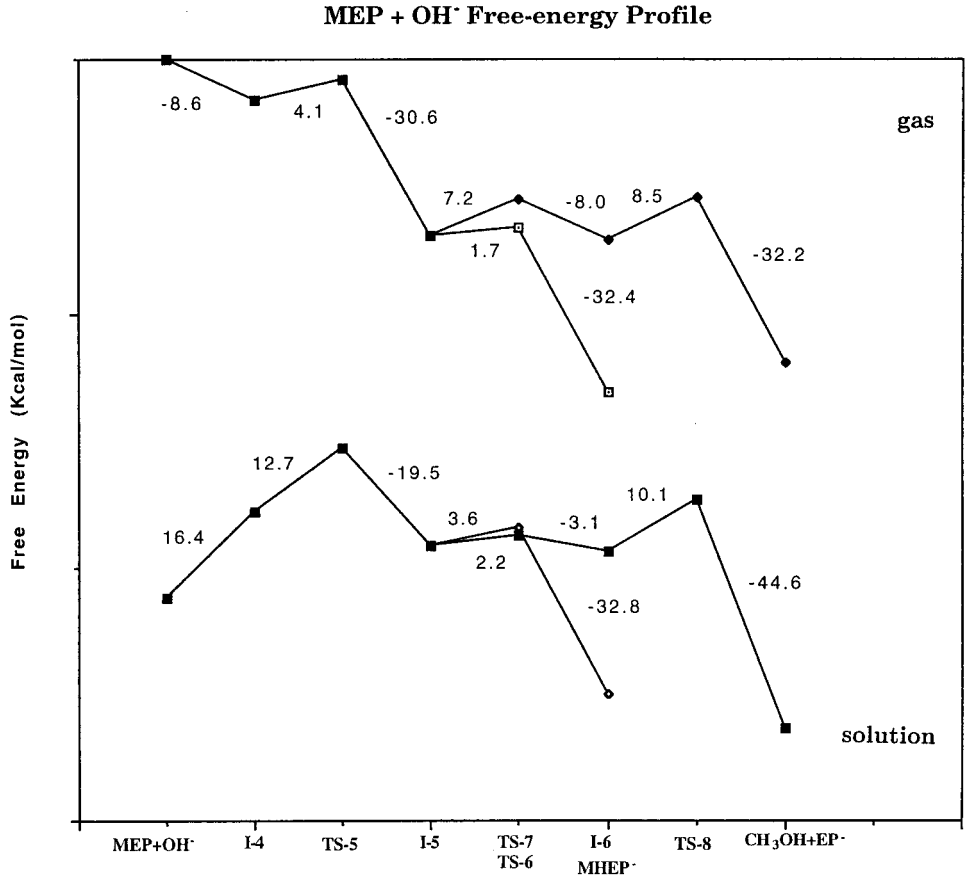

Figure 2. Relative MP2/6-31+G*//HF/6-31+G* activation free-energy profile for the gas-phase reaction of $(OH)^-$ with MEP (top) and the change in profile upon solvation (bottom). The zero of energy corresponds to the reactants at infinite separation. The numbers correspond to the free-energy differences of subsequent points.

Table 5. Relative Energies and Free Energies of the Rate-Limiting Transition States Located in the Gas Phase and in Solution Using CDM and PSGVB Solvation Free Energies for Reactions 1−3 at 298 K with Respect to the Reactants Separated at Infinity in the Gas Phase (All Energies Are Reported to 1 Decimal Place in kcal/mol)

		kcal/mol						
reaction	P−O^H (Å)	$\Delta E^{\ddagger}$[a]	$\Delta\delta E^{\ddagger}(T)$[b]	$T\Delta S^{\ddagger}$[c]	$\Delta G^{\ddagger}_{gas}$[d]	ΔG_s(TS)	ΔG_s(GS)	$\Delta G^{\ddagger}_{sln}$[e]
TMP + $(OH)^-$	2.76[f]	−20.8	2.3	−10.9	−7.6	−61.4[h]	−105.0[h]	36.0
	2.48[g]	−21.7	2.3	−10.9	−8.5	−58.3[h]	−105.0[h]	38.2
	2.30[g]	−24.6	2.3	−10.9	−11.4	−60.9[i]	−108.5[i]	36.2
MEP + $(OH)^-$	3.12[f]	−15.0	1.2	−9.6	−4.3	−72.5[h]	−106.2[h]	29.6
	2.67[g]	−18.0	1.2	−9.6	−7.2	−69.0[h]	−106.2[h]	30.1
	2.54[g]	−20.3	1.2	−9.6	−9.6	−77.4[i]	−111.0[i]	24.0
MPP + $(OH)^-$	3.27[f]	−12.8	1.4	−10.7	−0.6	−73.7[h]	−105.9[h]	31.6
	2.52[g]	−16.2	1.4	−10.7	−4.1	−65.9[h]	−105.9[h]	36.0
	2.43[g]	−17.9	1.4	−10.7	−5.8	−73.9[i]	−110.3[i]	30.6

[a] MP2/6-31+G* energy relative to reactants separated at infinity in the gas phase. [b] ZPE + E_{trans} + E_{rot} + E_{vib} + PV of MP2/6-31+G*-optimized gas-phase transition state relative to reactants. [c] T*(S_{trans} + S_{rot} + S_{vib}) relative to reactants. [d] $\Delta G^{\ddagger}_{gas} = \Delta E^{\ddagger} + \Delta\delta E^{\ddagger}(T) - T\Delta S^{\ddagger}$. [e] Solution free energies computed using eq 1. [f] MP2/6-31+G*-optimized transition state located in the gas phase. [g] MP2/6-31+G*-optimized transition state located in solution. [h] CDM solvation free energies. [i] PSGVB solvation free energies.

Table 6. Energy Dependence of the Rate-Limiting Transition State for Reactions 1−3 on Geometry Optimization Level, Basis Set Size, and Treatment of Electron Correlation

theory level basis set	MP2[a] 6-31+G*	MP2[b] 6-31+G*	MP2[b] 6-311++G(3df,3pd)	MP4(SDQ)[b] 6-31+G*
$\Delta E^{\ddagger}$(**TS**−**1**)[c]	−20.1	−20.8	−19.8	−20.1
$\Delta E^{\ddagger}$(**TS**−**5**)[c]	−15.2	−15.0	−14.6	−14.8
$\Delta E^{\ddagger}$(**TS**−**9**)[c]	−13.4	−12.8	−13.0	*d*

[a] Geometries optimized at the HF/6-31+G* level. [b] Geometries optimized at the MP2/6-31+G* level. [c] Energy relative to reactants separated at infinity. [d] Energy did not converge even when 500 MB of memory was allocated for the MP4 calculation.

diequatorial ring transition states since the latter pathway yields thermodynamically unfavorable products, $(CH_3O)^-$ and hydrogen propylene phosphate, compared to the former.

Rate-Limiting Transition States. Effect of Electron Correlation. As shown in Figures 1−3, the rate-limiting transition states for the reaction of $(OH)^-$ at the phosphorus atoms of TMP, MEP and MPP in the gas phase and solution are **TS-1**, **TS-5**, and **TS-9**, respectively. Thus, the rate-limiting step in the three reactions studied here is $(OH)^-$ attack at the phosphorus atom, i.e., the nucleophilic addition step. For the HF/6-31+G* fully optimized **TS-1**, **TS-5**, and **TS-9** transition states, the P−O^H distances are 2.56, 2.91, and 2.76 Å, respectively, and the corresponding formation free energies in solution are 37, 29, and 34 kcal/mol. To include the effect of electron correlation in bond formation, the rate-limiting transition states were reoptimized at the MP2/6-31+G* level; the resulting energies and solvation free energies computed using the MP2/6-31+G* geometries and charges are listed in Table 5. The MP2/6-31+G* P−O^H distances for **TS-1**, **TS-5**, and **TS-9** located in the gas-phase are 2.76, 3.12, and 3.27 Å, respectively, and the solution activation free energies for the alkaline hydrolyses of TMP, MEP, and MPP are 36, 30, and 32 kcal/mol, respectively. Thus, inclusion of electron correlation has a significant effect on the geometry of the rate-limiting transition state, favoring an "earlier" transition state for all three reactions. This effect is most evident for the six-membered ring phosphorane transition state **TS-9**, where inclusion of electron correlation increased the P−O^H distance by 0.5 Å and, consequently, the solvation free energy became more favorable (by about 3 kcal/mol).

To assess the sensitivity of the MP2/6-31+G* results to the size of the basis sets and the level of theory used to estimate electron correlation, two single-point calculations were carried out at the MP2/6-311++G(3df,3pd) and MP4(SDQ)/6-31+G* levels using the MP2/6-31+G*-optimized geometries. The results, summarized in Table 6, show that the MP2/6-31+G*//HF/6-31+G*, MP2/6-31+G*, MP2/6-311++G(3df,3pd), and MP4(SDQ)/6-31+G* energies of the rate-limiting transition state relative to the reactants differ by less than 1 kcal/mol.

Relocation of Rate-Limiting Transition States in Solution. The effect of solvent may alter the location of the rate-limiting transition state in solution since the solvation free energy is expected to vary along the reaction coordinate, defined as the P−O^H distance. To account for this effect, a series of constrained optimizations at the MP2/6-31+G* level were carried out for P−O^H distances, ranging from 3.6 to 2.1 Å, in decrements of 0.1 Å; that is, the reaction coordinate was fixed at the specified value while the remaining degrees of freedom were fully optimized. Since a constrained optimized structure is not a "true" saddle point, vibrational frequencies cannot be determined; thus, the gas-phase free energy was computed assuming the zero-point energy, vibrational energy, and vibrational entropy of the fully optimized gas-phase rate-limiting transition state. The solvation free energy of each constrained optimized structure was computed using either the continuum dielectric method or PSGVB/DelPhi programs (see Methods). (For the constrained optimized acyclic structures, the CDM solvation free energies were computed using two different radii for the hydroxyl hydrogen: the default value in Table 1 and a radius of 1.468 Å; the two sets of solvation free energies differ by less than 1 kcal/mol.) The gas-phase MP2/6-31+G* energies and solvation free energies of the constrained optimized structures were fitted to a ninth/tenth-order polynomial function,[42] and the fitted gas-phase energies and solvation free energies were subsequently used to compute the solution free energies. The variations in the gas-phase free energies, solvation free energies, and solution free energies along the reaction coordinate for the reactions of $(OH)^-$ with TMP, MEP, and MPP are depicted in Figures 4−6, respectively (the actual values are supplied in the Supporting Information). The maximum of ΔG_{sln} as a function of the reaction coordinate gave the location of the transition state in solution (see Table 5).

Figure 4 shows a distinct difference between the gas-phase free-energy profiles of the cyclic and acyclic molecules: the latter exhibits a weaker dependence on the P−O^H distance than the cyclic molecules because, relative to the reactant state, the pseudorotated cyclic intermediates, **I-5** and **I-8**, are more stable than the acyclic intermediate **I-2** (see Tables 2−4). For a fixed

(42) Press, W. H.; Flannery, B. P.; Teukolsky, S. A.; Vetterling, W. T. *Numerical Recipes. The Art of Scientific Computing*; Cambridge University Press: Cambridge, 1986.

Scheme 3. Schematic Diagram Depicting Fully Optimized HF/6-31+G* Structures for the Reaction of $(OH)^-$ at Phosphorus of MPP (MPP(P)) (Not All Transition States and Intermediates along the Pathways Are Depicted for the Sake of Clarity)

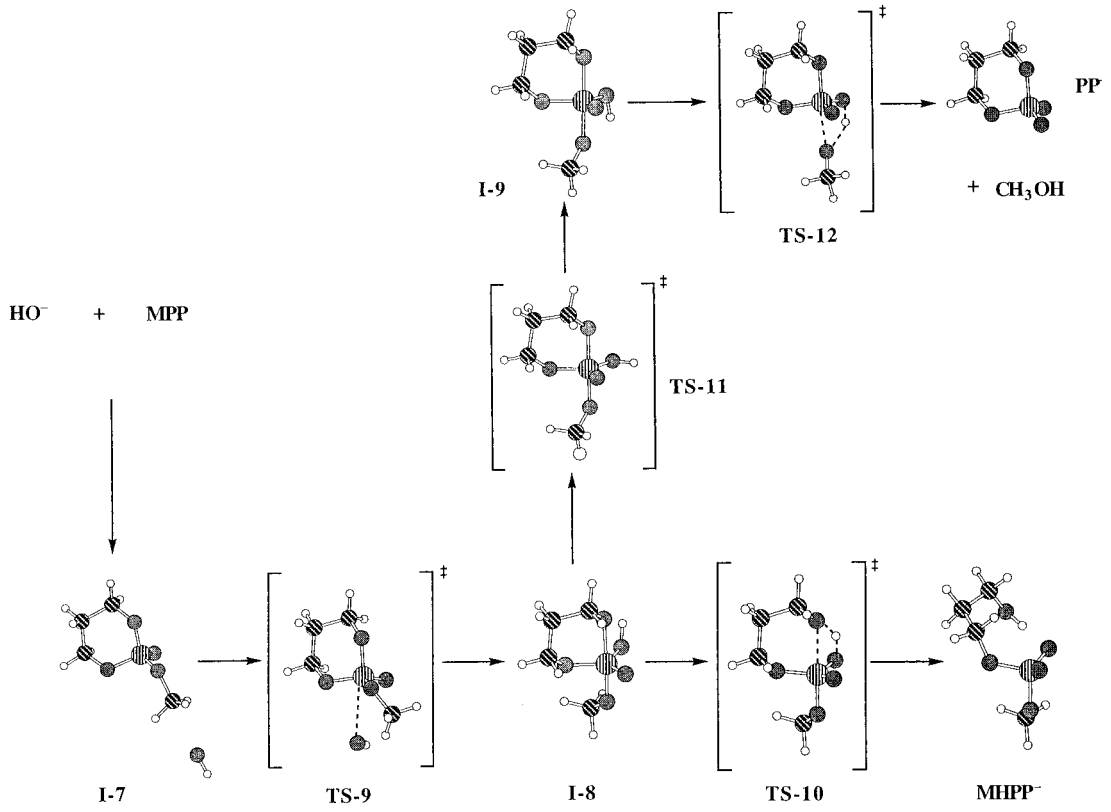

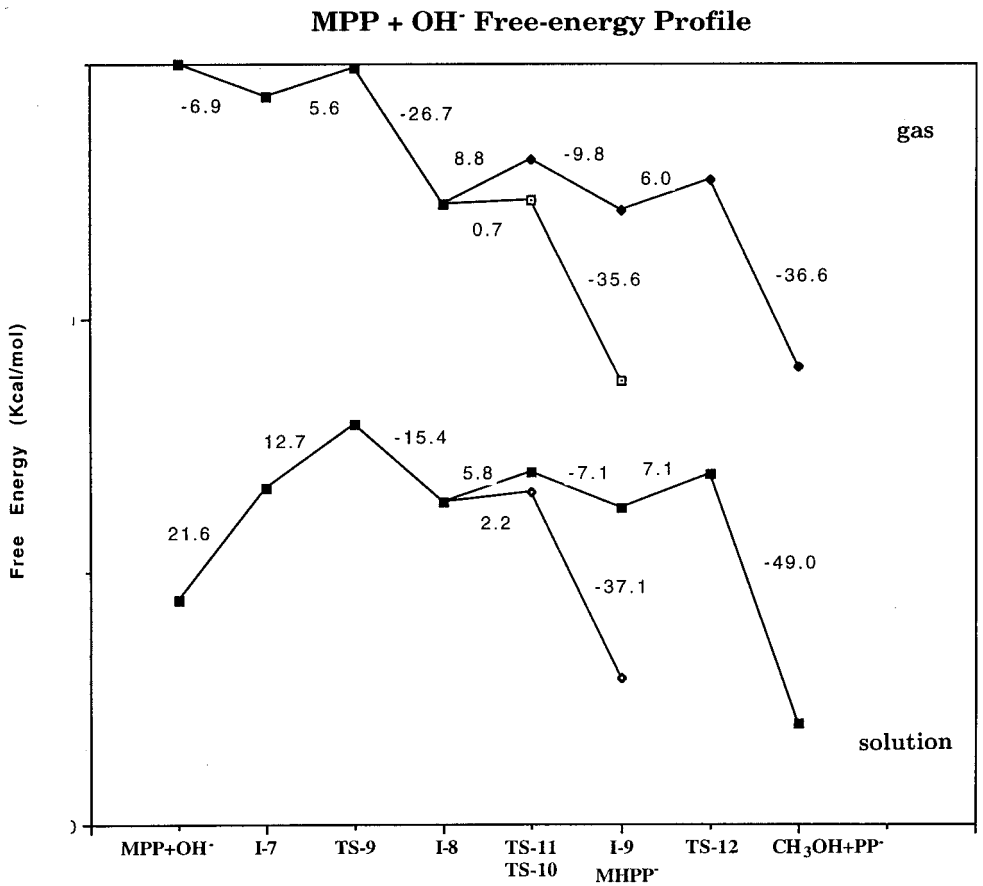

Figure 3. Relative MP2/6-31+G*//HF/6-31+G* activation free-energy profile for the gas-phase reaction of $(OH)^-$ with MPP (top) and the change in profile upon solvation (bottom). The zero of energy corresponds to the reactants at infinite separation. The numbers correspond to the free-energy differences of subsequent points.

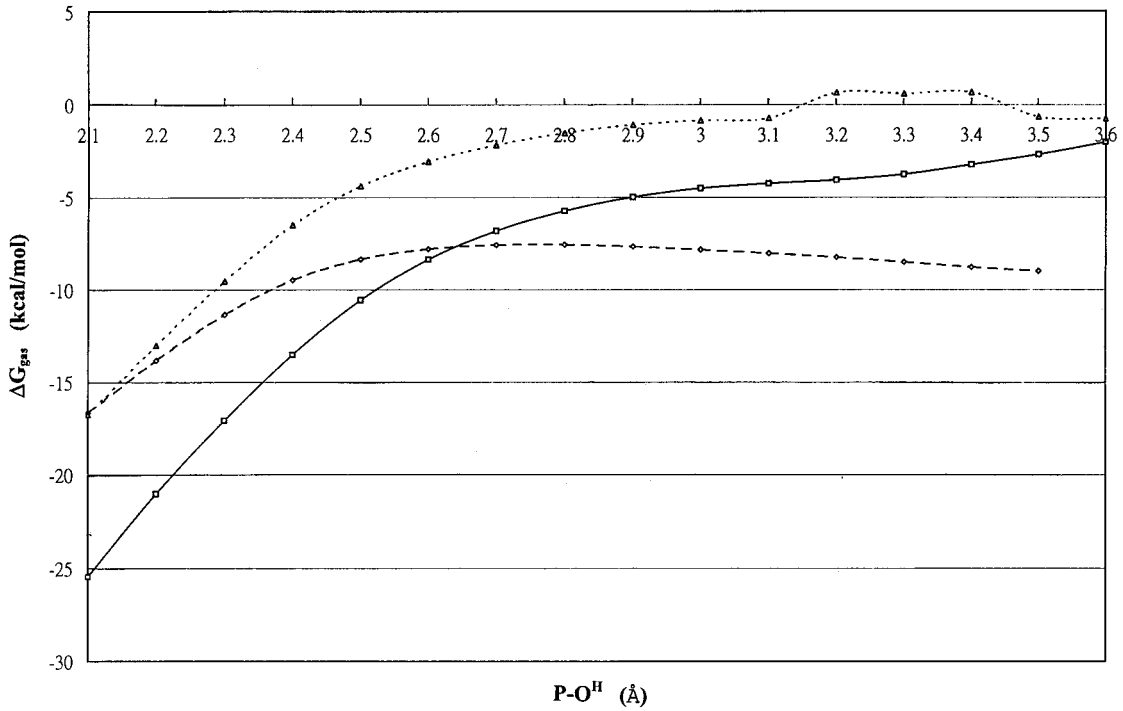

Figure 4. A comparison of ΔG_{gas} as a function of the P−O^H distance for the reactions of $(OH)^-$ with TMP (dashed line), MEP (solid line), and MPP (dotted line).

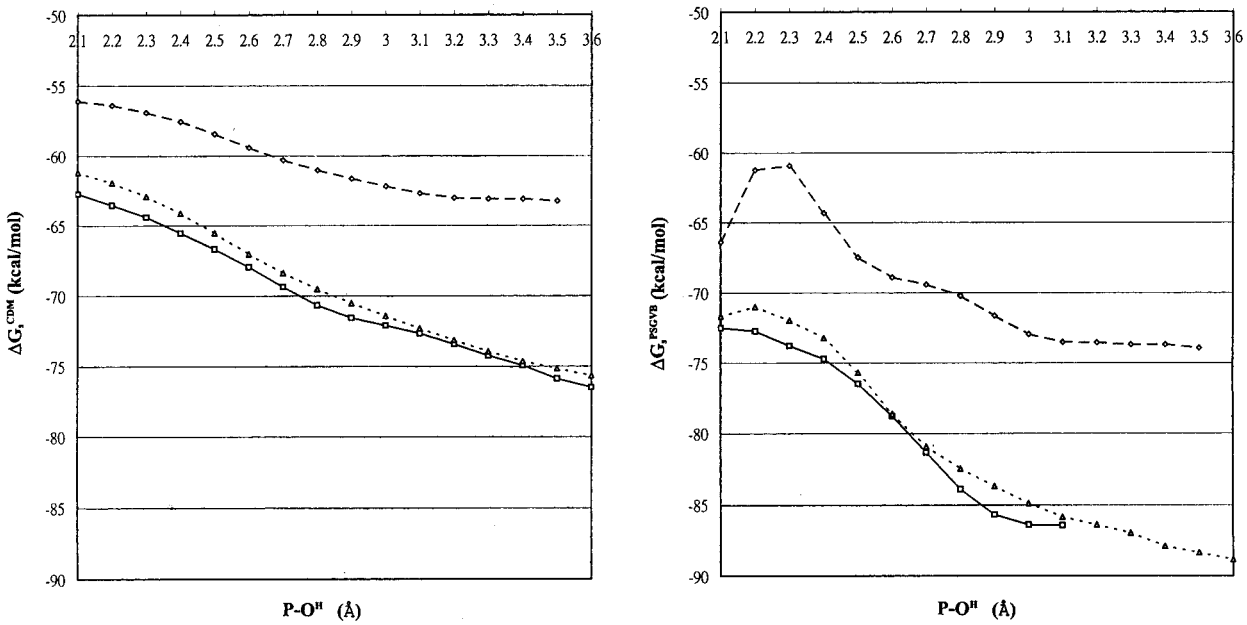

Figure 5. A comparison of CDM ΔG_s (left) and PSGVB ΔG_s (right) as a function of the P−O^H distance for the reactions of $(OH)^-$ with TMP (dashed line), MEP (solid line), and MPP (dotted line).

P−O^H distance, the gas-phase free energy of MEP···$(OH)^-$ is more favorable than that of the corresponding six-membered ring molecule, and as the P−O^H distance decreases, the gas-phase free energy of MEP···$(OH)^-$ drops more rapidly than that of MPP···$(OH)^-$. Figure 5 shows that at a given P−O^H distance, the cyclic molecules are better solvated than the acyclic counterpart; this is probably due to dihedral ring constraints yielding a more solvent-exposed hydroxyl group (compare the geometry of **TS-5** or **TS-9** with **TS-1**). Both five-membered and six-membered ring molecules exhibit a similar dependence of the solvation free energy on the reaction coordinate; however, for a fixed P−O^H distance, the solvation free energy of MPP···$(OH)^-$ is slightly more positive (by 1−2 kcal/mol) than that of the five-membered ring analog, reflecting the unfavorable electrostatic solvation of the extra hydrophobic methylene group in the six-membered ring. Figure 6 shows that, at a given P−O^H distance, the solution free energy of the acyclic molecule is greater than that of the cyclic molecules. This is mainly because the solvation free energy of the former is significantly less favorable than that of the latter, especially at a longer P−O^H distance (see Figure 5). On the other hand, the greater solution free energy of the six-membered cyclic molecule compared to its five-membered ring counterpart at a given P−O^H distance is largely due to the consistently higher gas-phase free energy of MPP···$(OH)^-$ relative to that of MEP···$(OH)^-$ (see Figures 4−6).

In each of the three reactions, the rate-limiting transition state in solution is located at a shorter P−O^H distance relative to the

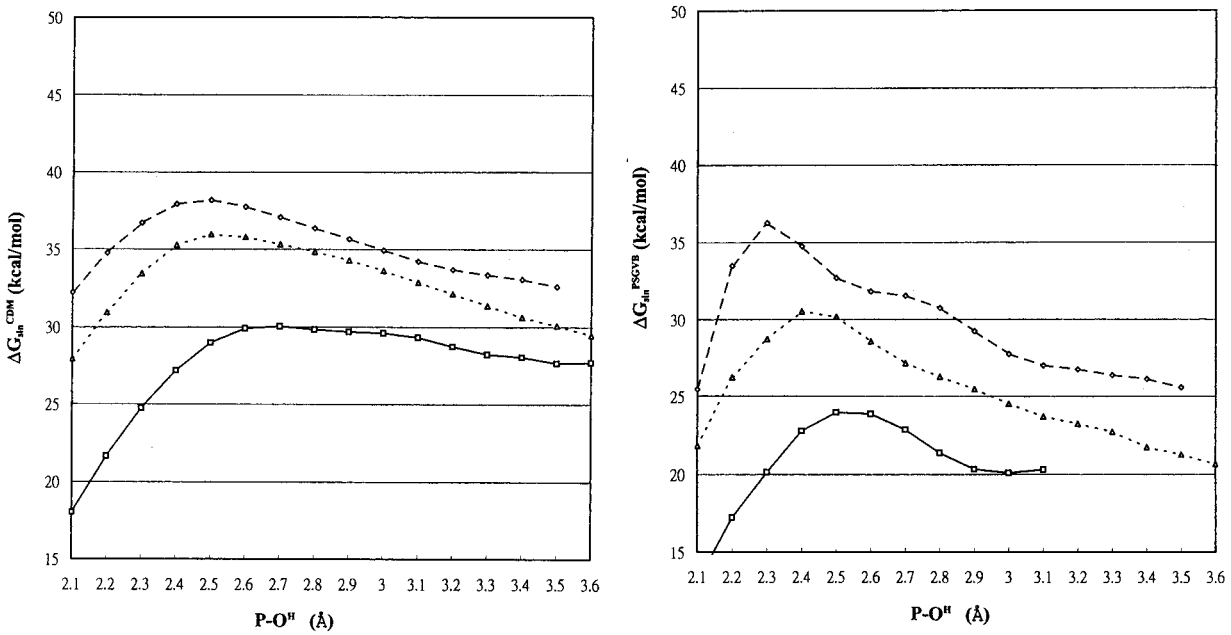

Figure 6. A comparison of ΔG_{sln} as a function of the P−O^H distance based on CDM ΔG_s (left) and PSGVB ΔG_s (right) for the reactions of $(OH)^-$ with TMP (dashed line), MEP (solid line), and MPP (dotted line).

gas-phase transition state: the P−O^H distances for **TS-1**, **TS-5**, and **TS-9** relocated using CDM solvation free energies decreased by 0.28, 0.45, and 0.75 Å, respectively, relative to the corresponding "gas-phase" distances. In contrast to the effect of electron correlation on the location of the rate-limiting transition states, the effect of solvent is to favor a "late" transition state because the magnitude of the solvation free energy increases as the P−O^H distance increases (see Figure 5). Consequently, the relocated rate-limiting transition states in solution are less well solvated and, hence, have higher solution activation free-energy barriers relative to the free energies corresponding to the "gas-phase" transition state (see Table 5). Figures 4−6 clearly show that the differential location of the five- and six-membered ring transition states stems from the different dependence of ΔG_{gas} (rather than ΔG_s) on the reaction coordinate.

Note that the two solvation models produce similar trends. The key difference between the two approaches is that the PSGVB ΔG_s are more negative than the CDM ΔG_s probably because the PSGVB ΔG_s includes the contribution to solvation free energy due to the polarization of the solute charge distribution by the surrounding water molecules (represented by a high dielectric continuum). Furthermore, for each of the relocated transition state in solution, the P−O^H distance based on the PSGVB ΔG_s is about 1−2 Å shorter than that based on the CDM ΔG_s.

Discussion

Product Distribution and Reaction Mechanism. Barnard and co-workers[43] demonstrated that in the reaction of TMP with ^{18}O-labeled hydroxide, one and only one labeled oxygen is incorporated into the product and exclusive P−O bond cleavage occurs. They proposed that a $S_N2(P)$ mechanism best fitted their observations, i.e., a concerted nucleophilic attack of the hydroxyl ion on the phosphorus with concomitant displacement of the methoxide. In contrast, Scheme 1 and Figure 1 show that alkaline hydrolysis of TMP does not proceed via a $S_N2(P)$ mechanism but is a multistep process in which the breakdown of the intermediate is much faster than its formation. If the breakdown of the intermediate is too rapid to allow exchange between the P−O bond and water, the multistep reaction in Scheme 1 would be indistinguishable from the one-step $S_N2(P)$ mechanism. Thus, the calculations have suggested an alternative mechanism that is consistent with the experimental observations.

(43) Barnard, P. W. C.; Bunton, C. A.; Llewellyn, D. R.; Vernon, C. A.; Welch, V. A. *J. Chem. Soc.* **1961**, 2670−2676.

Table 7. Experimental Activation Parameters (kcal/mol) for the Alkaline Hydrolyses of Acyclic TMP, Five-Membered Ring MEP, and 6-Membered Ring EPP at 298.15 K

molecule	$\Delta H^‡$	$T\Delta S^‡$	$\Delta G^‡$
TMP[a]	15.60 ± 0.2	−6.86 ± 0.3	22.46 ± 0.3
MEP[a]	7.80 ± 0.2	−6.86 ± 0.3	14.66 ± 0.3
EPP[b]	13.21	−8.74	21.94
TMP−MEP	7.8 ± 0.4	0.00 ± 0.6	7.80 ± 0.6
EPP−MEP	5.4 ± 0.4	−1.88 ± 0.6	7.29 ± 0.6

[a] Values are taken from ref 12. [b] Values are taken from ref 16. No errors were reported for the activation parameters obtained.

Kluger and co-workers[10] found negligible exocyclic cleavage in the alkaline hydrolysis of MEP (pH 8−11). To account for this, they assumed that the TBP MEP−$(OH)^-$ intermediate with the hydroxyl group axial is stable and undergoes ring-opening much faster than pseudorotation to **I-5**. In contrast, Scheme 2 and Figure 2 show that pseudorotation is not rate limiting and the TBP MEP−$(OH)^-$ intermediate with the hydroxyl group axial is unstable as it spontaneously pseudorotates to yield **I-5**. Since the free-energy barrier for exocyclic cleavage is greater (by 6.5 kcal/mol) than that for endocyclic cleavage, negligible amounts of exocyclic cleavage products are predicted, in accord with the experimental observations. In analogy to that of MEP, the alkaline hydrolysis of MPP is predicted to yield mainly the ring-cleavage product, methyl hydroxy propyl phosphate, with retention of configuration. Unfortunately, the products for the hydrolysis of MPP reaction in dilute alkali have not been reported, to our knowledge.

Free Energy Barriers and Reaction Rates. The experimentally-derived activation free energies (Table 7) for the reactions of $(OH)^-$ with TMP (22.5 kcal/mol),[12] MEP (14.7 kcal/mol),[12] and six-membered ring ethyl propylene phosphate, EPP

Table 8. Intra- and Intermolecular Contributions to the Rate Acceleration of Five-Membered Ring MEP Relative to Its Acyclic and Six-Membered Ring Analogs (All Energies Are Reported to 1 Decimal Place in kcal/mol)

	TMP−MEP			MPP−MEP		
a	*b,d*	*c,d*	*c,e*	*b,d*	*c,d*	*c,e*
$\Delta\Delta E^{\ddagger}$	−5.8	−3.8	−4.2	2.3	1.8	2.5
$\Delta\Delta\delta E^{\ddagger}$(T)	1.1	1.1	1.1	0.2	0.2	0.2
$\Delta(T\Delta S^{\ddagger})$	−1.3	−1.3	−1.3	−1.1	−1.1	−1.1
$\Delta\Delta G^{\ddagger}_{gas}$	−3.3	−1.3	−1.8	3.6	3.1	3.8
$\Delta\Delta G_s$(TS)	11.1	10.7	16.4	−1.2	3.1	3.5
$\Delta\Delta G_s$(GS)	1.3	1.3	2.5	0.3	0.3	0.7
$\Delta\Delta G^{\ddagger}_{sln}$	6.5	8.1	12.2	2.1	5.9	6.6

[a] Ground state to rate-limiting transition state. [b] Energies and free energies corresponding to gas-phase rate-limiting transition state. [c] Energies and free energies corresponding to relocated rate-limiting transition state in solution. [d] Solvation free energies computed using the continuum dielectric method. [e] Solvation free energies computed using combined PSGVB/DelPhi programs.

(21.9 kcal/mol)[16] are significantly less than the computed values in Table 5 after relocation of the rate-limiting transition state in solution. This is mainly because the solvation free energies of $(OH)^-$ ion, the monoanionic rate-limiting transition states, and the neutral reactants differ by an order of magnitude and the nonelectrostatic contributions to the solvation free energy have been neglected; thus, the errors involved in calculating the absolute solvation free energies are probably different and do not cancel when evaluating the solution activation free energies. In contrast, the error in the activation free-energy difference between the alkaline hydrolyses of two similar phosphoesters is expected to be smaller than the error in the individual activation free energy. This is because in taking the free-energy difference between two similar neutral ground states or two similar TBP monoanionic transition states, any systematic errors in the relative gas-phase free energies (arising from the basis set employed and treatment of electron correlation) or in the relative solvation free energies (due to approximations inherent in the continuum treatment of water and the sets of partial charges and radii employed as well as the neglect of nonpolar contributions) are likely to cancel.[15,23]

Table 8 summarizes the activation free energy differences, $\Delta G^{\ddagger}_{sln}$(TMP−MEP) and $\Delta G^{\ddagger}_{sln}$(MPP−MEP), based on the "gas-phase" rate-limiting transition states, and "solution-phase" transition states located using CDM and PSGVB ΔG_s. The activation free-energy difference between the alkaline hydrolyses of TMP and MEP, $\Delta G^{\ddagger}_{sln}$(TMP−MEP), computed using CDM ΔG_s, is 6.5 kcal/mol for the "gas-phase" transition state and 8.1 kcal/mol for the relocated transition state in solution; the latter is in accord with the measured difference of 7.8 ± 0.6 kcal/mol. However, the free-energy difference computed using PSGVB ΔG_s, 12.2 kcal/mol, overestimates the measured difference (by about 4 kcal/mol). In contrast, the "gas-phase" rate-limiting transition states for the base hydrolyses of MPP and MEP yield a $\Delta G^{\ddagger}_{sln}$(MPP−MEP) difference of only 2.1 kcal/mol, which significantly underestimates the rate acceleration of MEP base hydrolysis relative to that of MPP. However, upon relocation of the transition states in solution, the resulting $\Delta G^{\ddagger}_{sln}$(MPP−MEP) difference, 5.9 kcal/mol using CDM ΔG_s or 6.6 kcal/mol using PSGVB ΔG_s, is in closer agreement with the estimated difference of 7.3 ± 0.6 kcal/mol for the alkaline hydrolysis of ethyl propylene phosphate relative to that of MEP (see Table 8).

MEP versus TMP. Table 8 gives the intramolecular solute-solute and intermolecular solute−solvent contributions to the enhanced alkaline hydrolysis rates of five-membered ring MEP relative to its acyclic and six-membered ring analogs. The negative ΔE difference for the gas-phase reaction of $(OH)^-$ with TMP(P) relative to that with MEP(P) indicates that the activation energy for the $(OH)^-$ + TMP(P) reaction is less than that for the $(OH)^-$ + MEP(P) reaction. Ab initio ring strain energy calculations[44] suggest that this is because the five-membered ring has strain in the ground state as well as in the rate-limiting transition state, but the strain energy in the five-membered cyclic transition state is greater than that in the five-membered ring ground state. In other words, the destabilization of the five-membered ring transition state relative to its acyclic counterpart is greater than that of MEP relative to TMP. The negative ΔE difference is partially offset by a greater entropy loss in forming the acyclic transition state **TS-1** relative to the five-membered cyclic one **TS-5**. The net $\Delta G^{\ddagger}_{gas}$ difference remains negative but small (about −1 to −2 kcal/mol), indicating that reaction of $(OH)^-$ at TMP(P) is competitive with that at MEP(P) in the gas phase. Both PSGVB and CDM ΔG_s values in Table 8 show that MEP and TMP have similar solvation free energies (differing only by 1.3−2.5 kcal/mol), but the five-membered ring transition state is much better solvated (by 11−16 kcal/mol) compared to its acyclic counterpart. As shown in previous work,[24,25] this is because the hydroxyl oxygen in the acyclic transition state **TS-1** is less solvent-exposed than the hydroxyl oxygen in the cyclic transition state **TS-5**. (Note that the MP2/6-31+G* CHelpG charge on the hydroxyl oxygen for the acyclic and cyclic relocated transition states, −1.06*e* and -1.17*e*, respectively, are similar.) The differential solvation of the rate-limiting transition states reverses the order of reactivity in the gas phase such that the free-energy barrier for the alkaline hydrolysis of MEP is significantly smaller than that of TMP.

Thus, the origin of the million-fold enhanced rate of alkaline hydrolysis of five-membered ring MEP relative to TMP is solvent stabilization of the cyclic rate-limiting transition state relative to its acyclic counterpart. This is in accord with the conclusions arrived by Karplus and co-workers[24] (see Introduction). The present work and ring strain calculations[44] do not support the hypothesis that the rate acceleration of five-membered cyclic phosphate esters is due to relief of ring strain in the rate-limiting transition state. The calculations also do not support the hypothesis that part of the rate enhancement of five-membered cyclic phosphorus esters is due to steric crowding in the acyclic transition state compared to the cyclic one.[20] This assumes that the orientations of the two methyl groups in the acyclic and cyclic transition states are similar (see Figure 3 in ref 20), an assumption that is not found to be valid as evident from the methyl and methylene group orientations in **TS-1** and **TS-5**, respectively.

MEP versus MPP. In contrast to the reaction of $(OH)^-$ with MEP versus TMP, both $\Delta E^{\ddagger}$ and $\Delta G^{\ddagger}_{gas}$ are positive, indicating that $(OH)^-$ reacts faster at MEP(P) than at MPP(P) in the gas phase, similar to the behavior in solution. Ring strain calculations[44] suggest that the positive ΔE results from greater strain energy in the five-membered ring ground state compared to the five-membered cyclic transition state, i.e., the destabilization of MEP relative to MPP is greater than that of **TS-5** relative to **TS-9**. Hydroxide attack at MPP(P) is also retarded by a greater entropy loss, so that the net $\Delta G^{\ddagger}_{gas}$ intramolecular term contributes to roughly half of the observed rate acceleration. Table 8 shows that the remaining difference stems from the more favorable solvation of the five-membered ring transition state relative to its six-membered ring analog due to the relocation of the transition states in solution (see Results). In

(44) Dudev, T.; Lim, C. Submitted for publication.

other words, if the rate-limiting transition state in solution is assumed to be the same as that found in the gas phase, the five-membered ring "gas-phase" transition state becomes less well solvated compared to its six-membered ring counterpart (by 1.2 kcal/mol), and the computed $\Delta G^{\ddagger}_{sln}$ difference (2.05 kcal/mol) is only 0.28 of the experimental estimate (7.29 kcal/mol).

Note that it is the differential location of the five- and six-membered cyclic transition states in solution that contributes to part of the observed rate acceleration. If the six-membered ring transition state was located at the same $P-O^H$ distance (2.7 Å) as the five-membered ring one, the solvation free energy of the six-membered TBP structure (−68.4 kcal/mol) is only 1 kcal/mol less favorable than that of its five-membered counterpart (−69.4 kcal/mol), due presumably to the unfavorable solvation of the additional small, nonpolar methylene group in the six-membered ring. As shown in Figures 4−6 (see also Results), the differential location of the five- and six-membered cyclic transition states in solution is *not* due to the different dependence of the solvation free energy as a function of the $P-O^H$ distance. Instead, it is due to the different dependence of the gas-phase free energies along the reaction coordinate for the two types of reactions, which, in turn, results from the fact that, relative to the reactant state, the five-membered cyclic intermediates, **I-5** and **I-6**, are more stable than their six-membered ring counterparts, **I-8** and **I-9** (see Tables 3 and 4). Furthermore, ring strain calculations[44] show that the five-membered cyclic intermediate has less strain than its six-membered ring analog. Thus, both the differential gas-phase formation free energies and differential solvation free energies of the rate-limiting transition states contribute to the rate acceleration of MEP versus MPP alkaline hydrolysis.

Conclusions

(1) For the alkaline hydrolysis of TMP, the lowest free-energy pathway is nucleophilic addition at phosphorus, followed by pseudorotation and subsequent elimination with simultaneous intramolecular proton transfer to yield $(DMP)^-$ and MeOH (Scheme 1 and Figure 1). On the other hand, for the alkaline hydrolysis of MEP or MPP, the lowest free-energy pathway is hydroxide attack at phosphorus concerted with pseudorotation, followed by ring-opening with simultaneous intramolecular proton transfer (Schemes 2 and 3 and Figures 2 and 3). For the three reactions studied, the lowest free-energy pathway in solution is similar to that found in the gas phase except that the ion−dipole minimum does not exist in solution.

(2) For the alkaline hydrolyses of TMP, MEP, and MPP, the rate-limiting step is not pseudorotation or P−O cleavage but $(OH)^-$ attack at the phosphorus atom, i.e., formation of a long-range transition state (**TS-1**, **TS-5**, and **TS-9**, respectively).

(3) There is a significant change in the transition-state geometry due to solvent effects. Such large changes have been observed in the Menshutkin reaction, $H_3N + CH_3Cl \rightarrow CH_3NH_3^+ + Cl^-$, where the transition state occurs much earlier in water than in the gas phase.[45] In contrast, for the reactions of hydroxide with TMP, MEP, and MPP, solvent effects favor a "late" transition state as the magnitude of the solvation free energy increases with increasing $P-O^H$ distance (see Figure 5). The trends seen here are expected for other nucleophilic substitution reactions involving a small, anionic nucleophile (like hydroxide) and a neutral substrate.

(4) The million-fold enhanced rate of alkaline hydrolysis of five-membered ring MEP relative to its acyclic TMP analog results mainly from dihedral ring constraints yielding a more solvent-exposed hydroxyl group and thus, greater solvent stabilization of the cyclic transition state relative to its acyclic counterpart.

(5) On the other hand, the enhanced rate of alkaline hydrolysis of five-membered ring MEP relative to its six-membered ring MPP counterpart results from both ground-state destabilization of MEP relative to MPP due to ring strain and transition-state stabilization of five-membered ring **TS-5** relative to six-membered ring **TS-9** due to the differential location of the transition states in solution.

Acknowledgment. We are grateful to D. Bashford, M. Sommer, and M. Karplus for the program used to solve the Poisson equation. We are indebted to C. Y. Liu for his help in fitting the data and Figures 4−6. N. Y. Chang is supported by the Institute of Biomedical Sciences, Academia Sinica, Taiwan. This work was supported by Academia Sinica, the National Science Council, and the National Center for High Performance Computing in Taiwan.

Supporting Information Available: Tables listing (a) electronic energies (in Hartrees) (b) electronic energies as a function of the $P-O^H$ distance relative to reactants, (c) CDM and PSGVB solvation free energies as a function of the $P-O^H$ distance, and (d) solution free energies based on the fitted electronic energies and solvation free energies as a function of the $P-O^H$ distance (6 pages). See any current masthead page for ordering information and Web access instructions.

JA9729802

(45) Gao, J.; Xia, X. *J. Chem. Soc.* **1993**, *115*, 9667.